impedance response of a thin film on an electrode: Deciphering the influence of the double layer capacitance

Oumaïma Gharbi, Mai T.T. Tran, Mark E. Orazem, Bernard Tribollet, Mireille Turmine, Vincent Vivier

IMPEDANCE RESPONSE OF A THIN FILM ON AN ELECTRODE: DECIPHERING THE INFLUENCE OF THE DOUBLE LAYER CAPACITANCE

Dr. Oumaïma GHARBI,[a] Dr. Mai T.T. TRAN,[a] Prof. Mark E. ORAZEM,[b] Dr. Bernard TRIBOLLET,[a] Dr. Mireille TURMINE,[a] Dr. Vincent VIVIER[a,*]

[a] *Sorbonne Université, CNRS, Laboratoire Interfaces et Systèmes Électrochimiques (LISE), 4 place Jussieu F-75005 Paris, France*

[b] *Department of Chemical Engineering, University of Florida, Gainesville, FL 32611*

ABSTRACT

The different contributions of the interfacial capacitance are identified in the case of passive materials or thin protective coatings deposited on the electrode surface. The method is based on a graphical analysis of the EIS results to determine both the passive-film capacitance in the high-frequency domain and the double-layer capacitance in the low-frequency domain.

The proposed analysis is shown to be independent of the physicochemical origins of the frequency dispersion of the interfacial capacitances which results, from an analysis point of view of the experimental results, in the use of a constant-phase element. However, for a correct evaluation of the thin-film properties such as its thickness, the high-frequency data must be corrected for the double-layer contribution. In particular, it is shown that if the double-layer capacitance gives a frequency-dispersed response, it is necessary to correct the high-frequency part for the double-layer CPE. This is first demonstrated on synthetic data and then used for the determination of the thickness of thin oxide film formed on Al in neutral pH solution.

Keywords: Constant phase element, Double layer capacitance, Electrochemical impedance spectroscopy, Electrochemistry, Interfacial capacitance.

corresponding author: vincent.vivier@sorbonne-universite.fr (ORCID ID: 0000-0001-5424-0083)

1. INTRODUCTION

Determination of the effective capacitance of a polarized interface remains a difficult challenge. In the case of the study of passive films or a thin proactive coating, it is usually assumed that the interfacial capacitance measured, which results from the sum of the impedances of the film and the double layer, is mainly governed by the dielectric contribution of the passive film since the latter is much smaller than that of the double layer. Such an approximation is easy to verify *a posteriori* when data analysis is performed assuming that each of the contributions is a capacitance and that the order of magnitudes for the double layer capacitance is between 10 to 50 µF cm^{-2} for a wide range of electrolyte concentrations and over a large potential window [1]. However, both the electrochemical impedance of passive film [2-5] and double layer relaxation [6-8] usually exhibit a non-ideal behavior, thus resulting in the use of constant-phase elements (CPE) to account for the distribution of dielectric properties of the interface [8-10] as well as experimental factors (position of the reference electrode, adsorption of impurities…) [11-13].

The use of a CPE facilitates fitting of experimental results, but the parameters obtained, Q and α, are difficult to use directly as it has been shown by Brug et al. [14]. The CPE is seen to be a mathematical trick for which the physical meaning is often not clearly expressed [15], thus limiting the use of this electrical element to a narrow frequency range. The effect of a CPE was clearly demonstrated in the case of Mott-Schottky analysis of passive films, for which the use of a single-frequency method for measuring the dielectric properties of the films led to a significant dispersion of results such as the estimated number of charge carriers or the oxide films properties [16-18]. The CPEs have also been used in a wide variety of electrochemical applications, for instance to account for the blocking behavior of electrodes in symmetrical cells [19] or for the characterization of transport properties contained within separators in energy storage devices [20], and for the for the characterization of the non-ideal behavior of polycrystalline electrodes in aqueous solutions [21, 22] as well as in ionic liquids [22]. The CPE is also widely used for modeling the impedance response of Li-ion batteries materials in which the complexity of the system is due to the number of interfaces involved in the entire electrochemical system [23, 24].

As a result, the physical description of the interface requires models that account for the CPE behaviors observed experimentally. In other words, the analysis of the impedance data involving CPEs should result in capacitances with a physical meaning, that is the dielectric properties of thin films must be consistent with the thickness of the material investigated, thin

film or coating [25-27], and the double-layer capacitance must also be in the range of the expected value for a polarized interface [28, 29].

Another important point is that the capacitance of the thin layer is directly related to its thickness [29], providing a unique way for measuring *operando* this value. Thus, different methods have been devised for the evaluation of the passive film thickness [2, 30], but most of them rely on assumptions that are often difficult to verify experimentally. We have recently shown that the analysis of impedance data by the representation of complex capacitances makes it possible to determine certain interface properties, especially thanks to the exploitation of the high-frequency domain [31-33]. In this work, a special attention has been paid to the graphical analysis of the experimental data in the different frequency ranges, including the low-frequency domain, in order to determine the values of the capacitances without resorting to fitting procedures involving complex functions. It will be shown that such an approach allows determination of the thickness of a thin layer at the interface, independently of the use of a CPE to describe the distribution of time constants.

2. EXPERIMENTAL

The working electrode consisted of an Al electrode (99.95% - Goodfellow) containing 50 ppm Fe and 100 ppm Si impurities, laterally insulated by a cataphoretic paint and an epoxy resin, exposing a surface area of 0.2 cm^2. The surface of the electrode was mechanically ground with silicon carbide paper up to 1200 grade, sonicated in distilled water, and dried with a stream of nitrogen gas. A saturated mercury sulfate electrode (MSE; E_{MSE} = 0.64 V/SHE) was used as the reference electrode, and a large area platinum mesh was used as the counter electrode. Sodium sulfate solutions (0.01 M) were prepared from analytical grade reagents using distilled water.

All electrochemical experiments were performed using a Gamry Ref600 workstation. EIS measurements were performed at the corrosion potential after two-hour immersion of the electrode in the electrolyte deaerated by sparged Ar gas. The sinewave perturbation amplitude was 10 mV peak-to-peak and 12 points per frequency decade were measured between 100 kHz and 10 mHz.

Simulations were performed using Matlab® software.

3. RESULTS AND DISCUSSION

The mathematical foundation presented in this section demonstrates that a CPE associated with the double-layer can be observed at low frequencies, thus enabling correction of the impedance data for the influence of the double-layer. A demonstration of the approach is presented using both synthetic and experimental data.

3.1. PHYSICAL DESCRIPTION OF THE INTERFACE

Let us assume the simple case of a thin film such as a passive film or an organic coating deposited on the electrode surface with no or a negligible electrochemical reaction on its surface. Figure 1a shows the electrical representation of such an interface in the case of a passive electrode immersed in an electrolyte in which Z_{film} represents the impedance of the passive film and the CPE in series with Z_{film} represents the properties of the electrode-electrolyte interface. It is worth noting that this general description is independent of the dielectric and electrochemical properties of the film. Thus, Z_{film} can represent a point-defect [34, 35] or similar [36, 37] model, a passive semiconducting film [4, 38], a thin film exhibiting a resistivity distribution [39, 40], or a thin film containing active organic inhibitors [41, 42]. For simplicity, the high-frequency dispersion due to the contribution of ohmic impedance [43-46] is disregarded in this article so as to focus on the different contributions of the interfacial capacitance in the high and low frequencies.
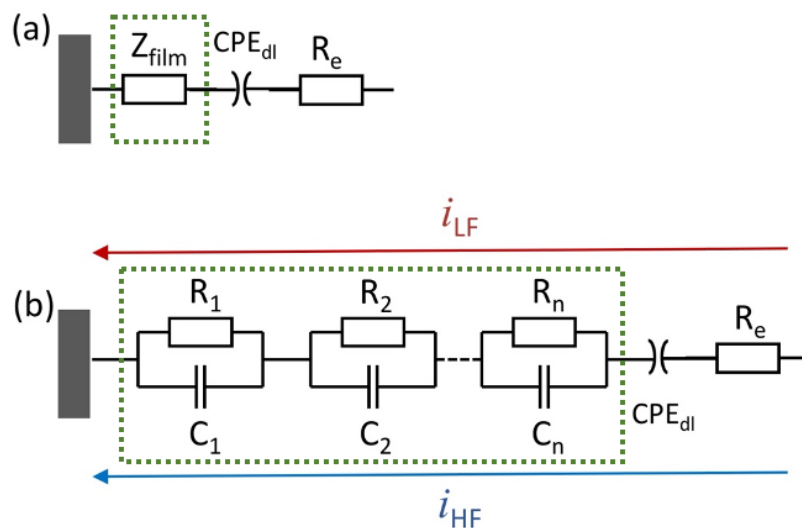

Figure 1: Electrical representation of the passive film interface (a) in the general case; (b) and using a decomposition in series of n Voigt elements for the thin film impedance

The use of a series of Voigt elements to account for the impedance of an electrode is possible for any impedance response that conforms to the Kramers-Kronig relationships [47, 48]. Thus,

the impedance contribution of the film can be described as a series of n Voigt elements, as shown in Figure 1b. Note that, as the CPE for the double layer is assumed to be known, the Voigt series accounts only for the impedance contribution of the film. Such an electrical equivalent circuit is of special interest when looking at low- and high-frequency limits for the impedance response of the interface. For any frequency, the current passes through the less resistive pathway. Thus, at high frequencies, the contribution of series capacitors dominates, and the limiting value of the impedance is given by

$$\lim_{\omega\to\infty} Z(\omega) = \sum_{k=1}^{n} \frac{1}{j\omega C_k} + \frac{1}{(j\omega)^{\alpha_{dl}} Q_{dl}} + R_e \qquad \textit{Eq. 1}$$

The first term of the right-hand side is the dielectric contribution of the film, C_{film}, and Eq. 1 may be expressed as

$$\lim_{\omega\to\infty} Z(\omega) = \frac{1}{j\omega C_{\text{film}}} + \frac{1}{(j\omega)^{\alpha_{dl}} Q_{dl}} + R_e \qquad \textit{Eq. 2}$$

Similarly, at low frequencies, the contribution of series resistances dominates, and the limiting value of the impedance is given by

$$\lim_{\omega\to 0} Z(\omega) = \sum_{k=1}^{n} R_k + \frac{1}{(j\omega)^{\alpha_{dl}} Q_{dl}} + R_e = R_{\text{film}} + \frac{1}{(j\omega)^{\alpha_{dl}} Q_{dl}} + R_e \qquad \textit{Eq. 3}$$

Eq. 3 shows that the double-layer capacitance can be obtained from the low-frequency domain. Then, the high-frequency limit (Eq. 2) allows calculation of the capacitance of the thin film. It is worth mentioning that, in this case, it is not necessary to make any assumption about the order of magnitude of each of the capacitances as usually done in the literature.

To illustrate the interest of this description in terms of electrical equivalent circuit of the interface, a preliminary study based on the analysis of synthetic data is first presented in the following. This approach allows us, not only to have data for which it will be simpler to present the approach we propose, but also to make simulations in frequency domains that are difficult to access experimentally in order to show the advantages and the limitations of this analysis. Then, experimental results obtained on a pure Al electrode will be discussed.

3.2. SYNTHETIC DATA

Let us assume that the power-law model accounting for a resistivity distribution along the thickness of the oxide film [49, 50] allows the description of the impedance response of the electrode. Thus, the impedance of the film may be expressed as

$$Z_{film}(\omega) = \int_0^\delta \frac{\rho(x)}{1 + j\omega\varepsilon\varepsilon_0\rho(x)}dx \qquad \text{Eq. 4}$$

in which δ is the thickness of the thin film, ε the material dielectric constant, ε_0 the vacuum permittivity ($\varepsilon_0 = 8.8542 \ 10^{-14}$ F cm^{-1}), and $\rho(x)$ the resistivity distribution inside the film, which is expressed as a function of the normal coordinate to the film, x, as

$$\rho(x) = \rho_\delta \left[\frac{\rho_\delta}{\rho_0} + \left(1 - \frac{\rho_\delta}{\rho_0}\right)\left(\frac{x}{\delta}\right)^\gamma \right]^{-1} \qquad \text{Eq. 5}$$

where ρ_0 (Ω cm) and ρ_δ (Ω cm) are the boundary values of the resistivity at the metal/film interface and at the film/solution interface, respectively, and γ is a constant indicating the extent of the variation in resistivity. The value of ρ_0 and ρ_δ may vary to a large extent, depending on the system under investigation [50-52]. This impedance contribution was previously shown to be equivalent to a CPE on a restricted frequency domain delimited by the values of $f_0 = 1/2\pi\rho_0\varepsilon\varepsilon_0$ and $f_\delta = 1/2\pi\rho_\delta\varepsilon\varepsilon_0$ [49, 50].

Moreover, the double-layer capacitance always exists and is in series with the capacitance of the film. A typical value for the double layer is expected to be in the range of 10 to 50 µF cm^{-2}, but frequency dispersion ascribable to the geometry of both the electrode and electrochemical cell usually results in a CPE-like behavior of the double layer with the parameters Q_{dl} and α_{dl}. It was previously shown that the Brug relation for such a surface distribution of time-constants allows calculation of the double-layer capacitance from the CPE parameters [14, 30]. The capacitance may be expressed, in the case of a blocking electrode (i.e., when the charge transfer resistance is much larger than the electrolyte resistance), as

$$C_{dl} = (Q_{dl})^{1/\alpha_{dl}}(R_e^{-1})^{(\alpha_{dl}-1)/\alpha_{dl}} \qquad \text{Eq. 6}$$

where R_e is the electrolyte resistance.

The total impedance that can be measured at the working electrode is thus given by:

$$Z(\omega) = \int_0^\delta \frac{\rho(x)}{1 + j\omega\varepsilon\varepsilon_0\rho(x)}dx + \frac{1}{(j\omega)^{\alpha_{dl}}Q_{dl}} + R_e \qquad \text{Eq. 7}$$

Figure 2 shows synthetic data of typical impedance diagrams in Nyquist representation for a 5 nm thick oxide thin film as a function of the resistivity at the interface between the electrode and electrolyte. These simulations were performed with $Q_{dl} = 47\ 10^{-6}\ F\ s^{(1-\alpha dl)}\ cm^{-2}$ and $\alpha_{dl} = 0.9$ corresponding to a double layer capacitance of $20\ \mu F\ cm^{-2}$ (calculated with Eq. 6).

Figure 2 highlights two time-constants that are characteristic of a CPE in the low-frequency domain and the thin film impedance in the high-frequency domain. The latter is more or less well defined (Figure 2b) since the low-frequency part of the impedance of the thin film overlaps the high and medium-frequency contributions of the double layer capacitance, the extent of overlap depending on the value of ρ_δ. The use of different graphical representations allows a better visualization of the different time constants. Figure 3 shows the Bode representation of the electrolyte resistance-corrected data for simulations carried out with the same parameters as in Figure 2. These data were obtained by subtracting the R_e value (determined as the high-frequency limit of the real part of the impedance) to the EIS data. The variation of the impedance modulus as a function of frequency (Figure 3a) clearly illustrates the CPE behavior of the double layer in the low-frequency range ($\alpha < 1$); whereas, the impedance response in the medium- and high-frequency domains, depends on ρ_δ.

Figure 3b shows the variation of the phase angle corrected from the electrolyte resistance. In the low-frequency domain, all the curves superimpose at a constant value of -81°, which corresponds to the contribution of the double layer relaxation ($\alpha_{dl} = 0.9$).

In the high-frequency domain, the value of the phase tends towards -90°, but, at this point, it is worth noting that depending on the value of ρ_δ, it may be not possible to determine the high-frequency limit of the impedance. Indeed, for the smallest value of ρ_δ, the frequency domain should be enlarged to access the limiting value of the capacitance, which may be, from an experimental point of view, out of the range of the equipment capability.

In the intermediate-frequency range, i.e., for frequencies above 100 Hz (this value is determined by ρ_0) a plateau is observed which shows a slight variation of the phase angle and which could be wrongly interpreted as a CPE. Indeed, to analyze these data in more detail, the graph of the absolute value of the imaginary part (in a log-log scale) is presented as a function of frequency in Figure 4a for $\rho_\delta = 10^7\ \Omega\ cm$ and $\rho_0 = 10^{10}\ \Omega\ cm$. As expected, the low-frequency domain shows a linear variation allowing a slope of -0.9 to be obtained that corresponds to $-\alpha_{dl}$. In the high-frequency domain, the slope of the curve is -1, corresponding to the behavior expected for a pure capacitance. On this frequency domain, C_{film} can be determined. In the medium-

frequency domain, a quasi-linear variation of the curve is obtained over 2 decades of frequency, suggesting again a CPE-like behavior.
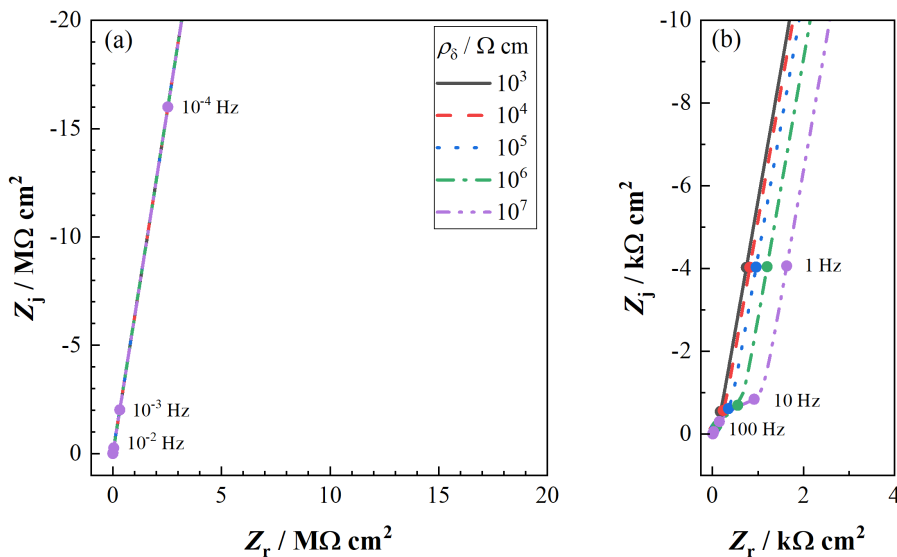

Figure 2: Nyquist representation of the impedance calculated for a passive film obeying to a power law model in series with a non-ideal double layer described by a CPE as a function of ρ_δ. (a) whole frequency plot; (b) zoom on the HF domain. Parameters used for the synthetic data: $\rho_0 = 10^{10}$ Ω cm, $\delta = 5$ nm, $\gamma = 4$, $\varepsilon = 10$, $R_e = 10$ Ω cm^2, $Q_{dl} = 47\ 10^{-6}$ F s$^{(1-\alpha)}$ cm^{-2}, $\alpha_{dl} = 0.9$.
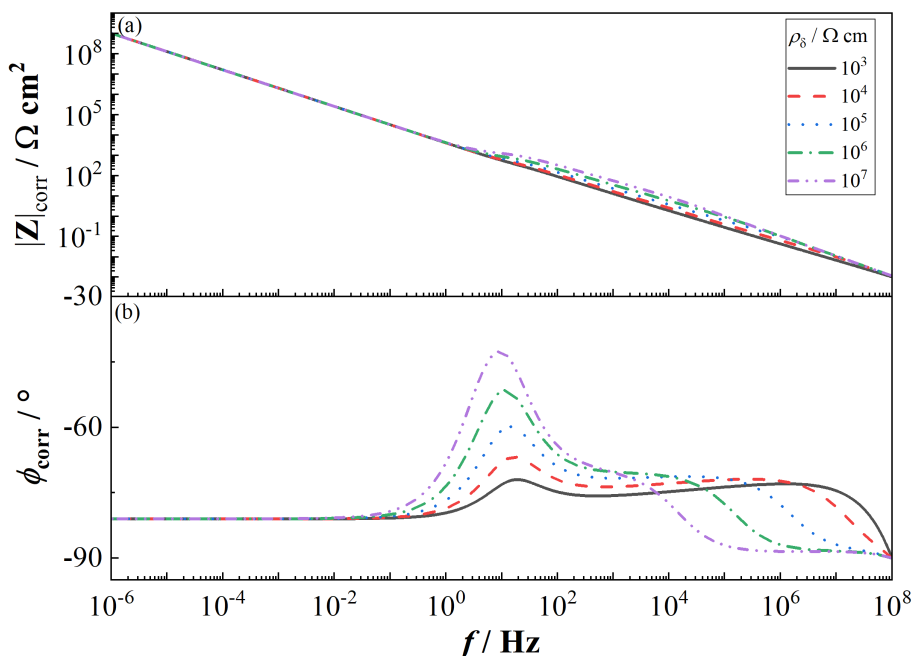

Figure 3: Bode representation of the impedance (adjusted from the electrolyte resistance) calculated for a passive film obeying to a power law model in series with a non-ideal double layer described by a CPE as a function of ρ_δ (a) impedance modulus; (b) phase angle corrected from the electrolyte resistance. Parameters used for the synthetic data: $\rho_0 = 10^{10}$ Ω cm, $\delta = 5$ nm, $\gamma = 4$, $\varepsilon = 10$, $R_e = 10$ Ω cm^2, $Q_{dl} = 47\ 10^{-6}$ F s$^{(1-\alpha)}$ cm^{-2}, $\alpha_{dl} = 0.9$.
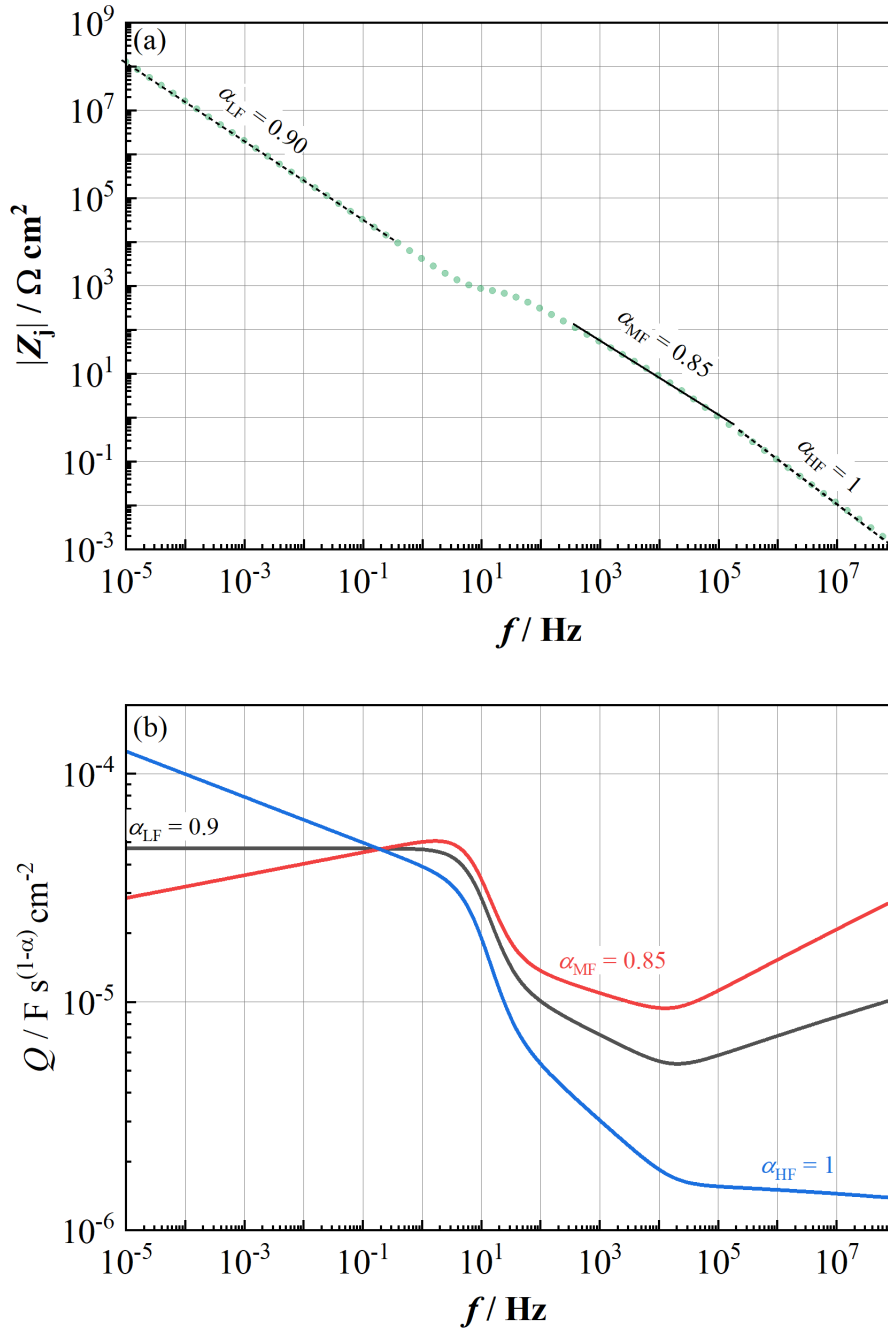
Figure 4: Graphical analysis of the impedance calculated for a passive film obeying to a power law model in series with a non-ideal double layer described by a CPE. (a) variation of the absolute value of the imaginary part of the impedance as a function of the frequency; (b) variation of the parameter Q of the CPE for the different values of α determined in Graphic a. Parameters used for the synthetic data: $\rho_0 = 10^{10}$ Ω cm, $\rho_\delta = 10^7$ Ω cm, $\delta = 5$ nm, $\gamma = 4$, $\varepsilon = 10$, $R_e = 10$ Ω cm^2, $Q_{dl} = 47$ 10^{-6} F s$^{(1-\alpha)}$ cm^{-2}, $\alpha_{dl} = 0.9$.

The frequency-dependent value of the CPE parameter Q can be calculated using the values of α determined graphically according to the relationship

$$Q = \frac{-1}{Z_j \times \omega^\alpha} \times \sin\left(\frac{\alpha\pi}{2}\right)$$

Eq. 8

Figure 4b shows the variations of Q as a function of frequency obtained for the three different values of α determined on Figure 4a. The low-frequency domain allows calculation of Q equal to 47 10^{-6} F $s^{(1-\alpha)}$ cm^{-2} for $\alpha = 0.9$, in perfect agreement with the value used for the simulation. On the other hand, the intermediate frequency domain does not show a constant Q value over the frequency range for which $\alpha = 0.85$ is observed. This is due to the fact that, over this range, two relaxations that can be described by CPEs take place, and the sum of two CPEs in series is not a CPE. In the high-frequency domain, the Q value for $\alpha = 1$ does not reach a plateau and varies slightly with frequency. A value of 1.5 µF cm^{-2} can be determined from the graph (Figure 4b) at 1 MHz. From the data used for generating synthetic data, the high frequency value of the interfacial capacitance consisted in the double layer capacitance (20 µF cm^{-2}) and the high frequency film capacitance $C_{film} = \varepsilon\varepsilon_0/\delta = 1.77$ µF cm^{-2} in series, thus $C = 1.63$ µF cm^{-2}. The high-frequency analysis results in 8% error in the evaluation of the static capacitance.

A similar analysis can be performed using the complex capacitance that can be obtained from the impedance data using the relationship [31]

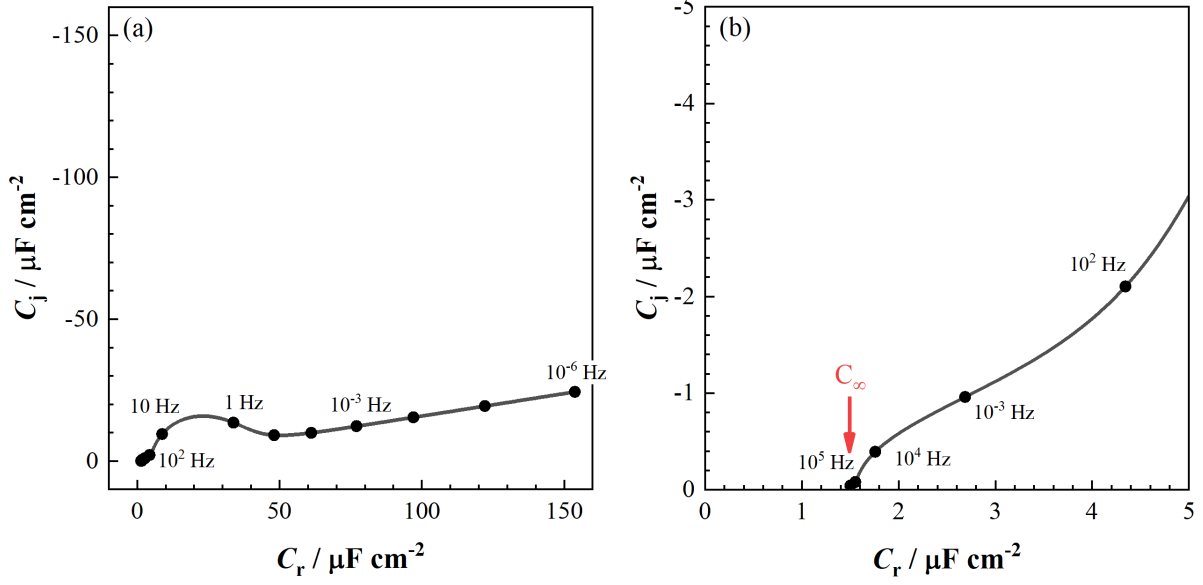$$C(\omega) = \frac{1}{j\omega(Z(\omega) - R_e)}$$

Eq. 9

Figure 5: Capacitance graph of the impedance calculated for a passive film obeying to a power law model in series with a non-ideal double layer described by a CPE. (a) whole frequency plot; (b) zoom on the HF domain. Parameters used for the synthetic data: $\rho_0 = 10^{10}\ \Omega$ cm, $\rho_\delta = 10^7\ \Omega$ cm, $\delta = 5$ nm, $\gamma = 4$, $\varepsilon = 10$, $R_e = 10\ \Omega$ cm^2, $Q_{dl} = 47\ 10^{-6}$ F s$^{(1-\alpha)}$ cm^{-2}, $\alpha_{dl} = 0.9$.

Figure 5 shows the capacitance graph of the impedance calculated for a passive film obeying a power law model in series with a non-ideal double layer described by a CPE. The system shown in Figure 5 corresponds to the system presented in Figure 2 for $\rho_\delta = 10^7\ \Omega$ cm. Here again, the extrapolation of the capacitance in the high frequency domain allows a value of C_∞ 1.5 µF cm^{-2} to be determined. However, if the actual double layer impedance can be obtained from the low frequency analysis, it is then possible to calculate the corrected impedance Z_{corr} of the passive film according to

$$Z_{corr}(\omega) = Z(\omega) - \frac{1}{(j\omega)^{\alpha_{dl}}Q_{dl}}$$

Eq. 10

and perform the same graphical analysis as before. The complex representation of the impedance (Figure 6) shows that the high frequency limit is 1.78 µF cm^{-2}, which is in agreement with the dielectric properties of the film calculated from its thickness and relative permittivity ($C_{film} = 1.77$ µF cm^{-2}). These results show that the interpretation of impedance data in the high-frequency domain remains a thorny issue. Indeed, the simple analysis in terms of equivalent circuit shows that one must obtain a capacitance in the high-frequency domain, but the fact that the capacitive response of the interface may be the result of CPE complicates the quantitative analysis and leads to errors.
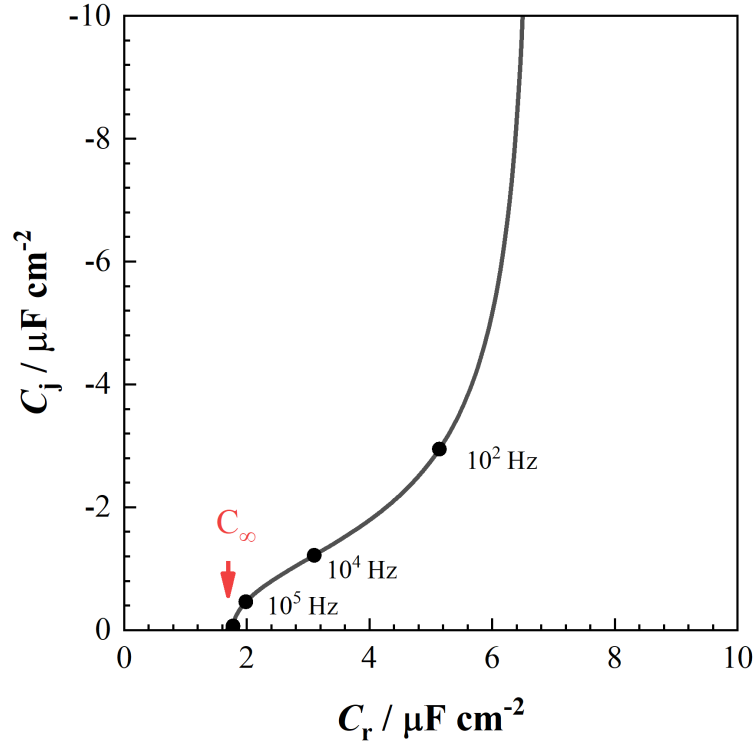
11

Figure 6: Capacitance graph of the impedance calculated for a passive film corrected from the CPE contribution of the double layer. Parameters used for the synthetic data: $\rho_0 = 10^{10}\ \Omega$ cm, $\rho_\delta = 10^7\ \Omega$ cm, $\delta = 5$ nm, $\gamma = 4$, $\varepsilon = 10$, $R_e = 10\ \Omega$ cm^2, $Q_{dl} = 47\ 10^{-6}$ F s$^{(1-\alpha)}$ cm^{-2}, $\alpha_{dl} = 0.9$.

The high-frequency capacitance value is often used to find out the properties of the passive film, e.g., its thickness if the relative permittivity of the material is known, according to the relation

$$C_{film} = \frac{\varepsilon \varepsilon_0}{\delta} \qquad\qquad Eq.\ 11$$

Figure 7 shows the thickness of the passive film determined from the graphical analysis of the impedance for synthetic data as a function of ρ_δ. The expected value for the film thickness is $\delta = 5$ nm, which was used as parameter for the calculation of the power law impedance contribution. If we assume that the double layer capacitance is negligible (blue curve), an assumption often found in the literature, the error made on the evaluation of the thickness is a function of ρ_δ and can reach 50% for the smallest value of ρ_δ. The same is true if the high-frequency capacitance is corrected by the infinite capacity obtained from the analysis of the CPE behavior of the double layer (red curve), the error can be as high as 45% in this case. In fact, Figure 7 shows that the only way to obtain a right thickness estimate is to correct the impedance of the CPE of the double layer before extrapolating the value of the high-frequency capacitance (black curve). This approach should be preferred (when data analysis allows it)

because the ρ_δ value is generally not known and it is then difficult to estimate the error with which the determination of δ is made.
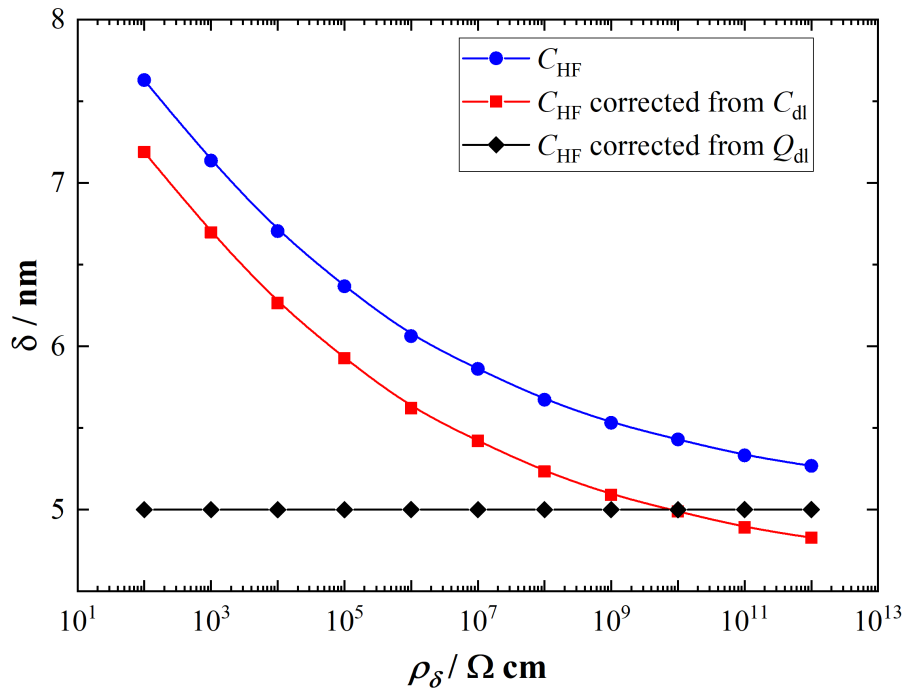

Figure 7: Evolution of the thin film thickness calculated assuming that the double layer is negligible (blue circles), by correcting the HF capacitance by the double layer capacitance (red squares) or by the double layer CPE (black diamonds) as a function of ρ_δ. Parameters used for the synthetic data: $\rho_0 = 10^{10}$ Ω cm, $\delta = 5$ nm, $\gamma = 4$, $\varepsilon = 10$, $R_e = 10$ Ω cm², $Q_{dl} = 47\ 10^{-6}$ F s$^{(1-\alpha)}$ cm², $\alpha_{dl} = 0.9$.

3.3. EXPERIMENTAL RESULTS ON ALUMINUM

Figure 8 shows the EIS diagrams of an Al electrode after two-hour immersion at the corrosion potential in a 0.01 M and 0.1 M Na₂SO₄ solutions. In both cases, the shape of the EIS diagrams clearly shows a CPE behavior in the high-frequency domain; whereas, the capacitive loop hides the double-layer capacitance contribution. The two main distinctions in these EIS diagrams are a decrease of electrolyte resistance for the more concentrated solution and a very slight shift in time-constant frequency. However, the Bode representation (Figure 9) shows the contribution of two time constants, as already observed [53]. In the 0.01 M Na₂SO₄ solution, the low-frequency domain allows measurement of a double layer CPE t($Q_{dl} = 35 \times 10^{-6}$ F s$^{(1-\alpha)}$ cm², α_{dl} = 0.89); whereas, in 0.1 M Na₂SO₄ solution, $Q_{dl} = 43 \times 10^{-6}$ F s$^{(1-\alpha)}$ cm² and $\alpha_{dl} = 0.90$, corresponding to a double-layer capacitance of 15.3×10^{-6} F cm² and 18.5×10^{-6} F cm² respectively, when using the Brug formula (Eq. 6). These values for different electrolyte concentrations are in agreement with reported data for the mercury electrode [1].
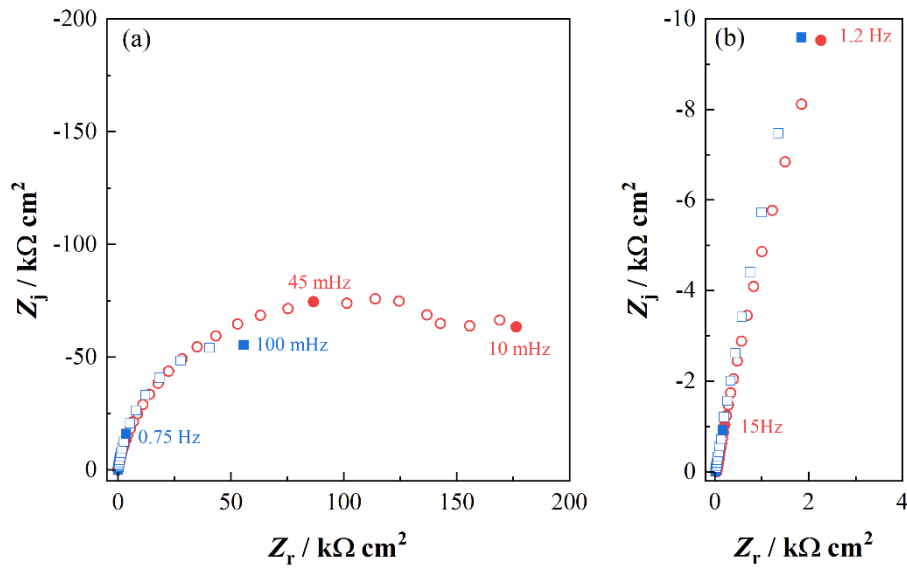
13

Figure 8: Nyquist representation of the impedance response of an Al electrode after 2-hour immersion in 0.01 M Na₂SO₄ deaerated solution at the corrosion potential (E_corr = -1.196 V/MSE) red circles; and in 0.1 M Na₂SO₄ solution blue squares. (a) whole frequency plot; (b) zoom on the HF domain.

In order to determine the thickness of the oxide film formed on the surface of the aluminum electrode, the complex capacitance was calculated from the impedance and from the corrected impedance by double layer CPE (Figure 10) by considering a permittivity value of 11.5. In the 0.01 M Na₂SO₄ solution, high-frequency extrapolation allows calculation of an infinite capacitance of 1.06×10^{-6} F cm^{-2} in the case of raw data and 1.4×10^{-6} F cm^{-2} in the case of corrected data, i.e., a film thickness of 9.6 nm and 7.3 nm, respectively. Interestingly, if the infinite capacitance is corrected with the value of the double-layer capacitance determined with the Brug formula, an intermediate value of the thickness is obtained (8.9 nm). In the 0.1 M Na₂SO₄ solution, high-frequency extrapolation allows calculation of an infinite capacitance of 1.13×10^{-6} F cm^{-2} in the case of raw data and 1.6×10^{-6} F cm^{-2} in the case of corrected data, leading to a film thickness of 6.3 nm for the corrected data. These results show that the direct use of the infinite capacitance to determine the thickness of the passive layer can lead to an error of about 20%, while the correction with the double-layer capacitance determined from the Brug relation, as proposed in reference [53], reduces the error to about 10%, the ideal being to adjust the impedance by the double layer CPE before calculating the thickness.

The thickness values determined in this work are within the range of those encountered in the literature for various thin oxide films on Al[53] or steel[52], but are larger than those reported in Evertsson et al.[54] using EIS, XPS and XRR. However, the formula used in this article to analyze EIS data is equivalent to that developed by Hsu and Mansfeld[55] which was shown to underpredict the film thickness for an oxide on 18 Cr-8Ni steel[9] by a factor of about 10

compared to values obtained by surface analysis. Moreover, this discrepancy between our data and those of Evertsson et al. may stem from the actual value of the dielectric constant. A value between 7.5 to 15 has been reported in the literature[56] leading to thicknesses between 4.1 and 9.5. This range is in agreement with our results and those of Evertsson et al. thus showing that EIS is an effective tool to control the thickness of the thin oxide film formed on the electrode surface assuming the permittivity of the material is known.
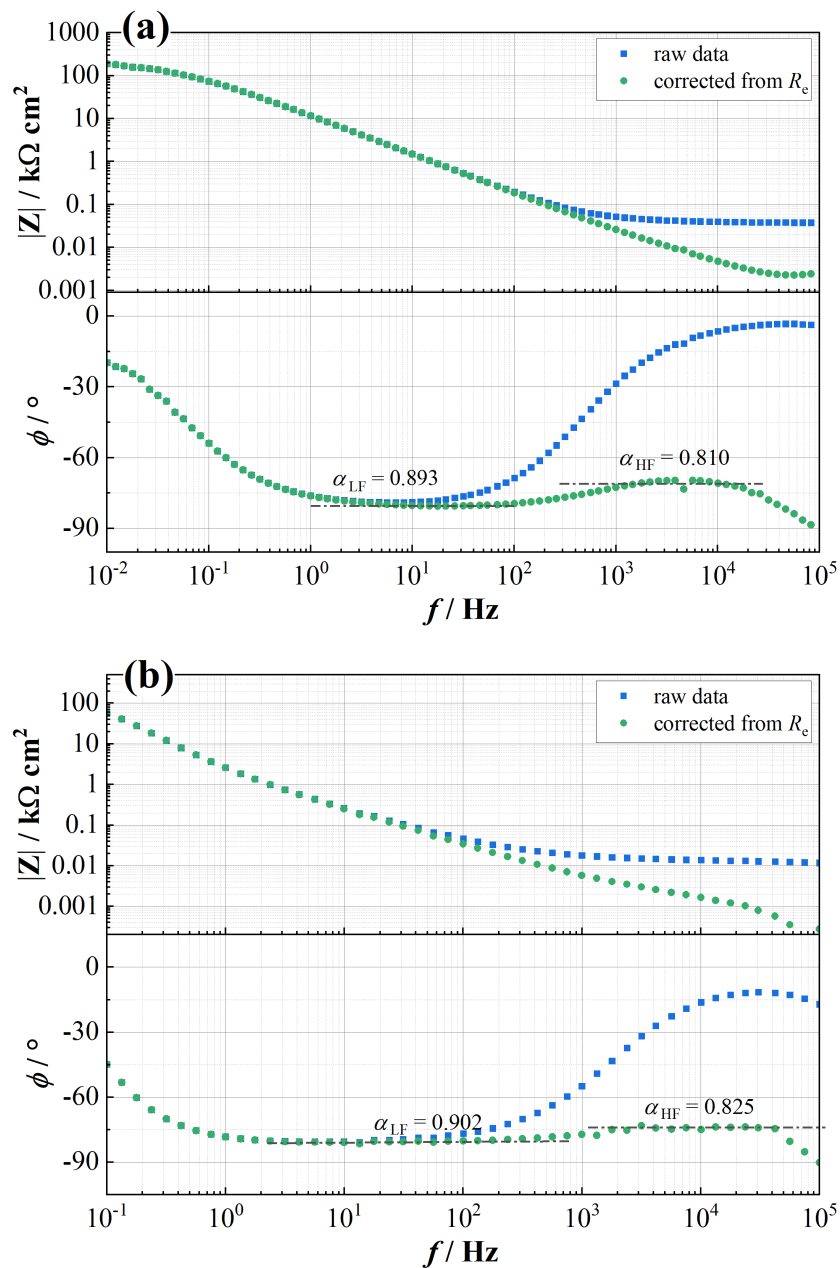

Figure 9: Bode representation of the impedance response of an Al electrode after 2-hour immersion in 0.01 M Na₂SO₄ deaerated solution at the corrosion potential (E_corr = -1.196 V/MSE) panel (a); and in 0.1 M Na₂SO₄ solution panel (b).
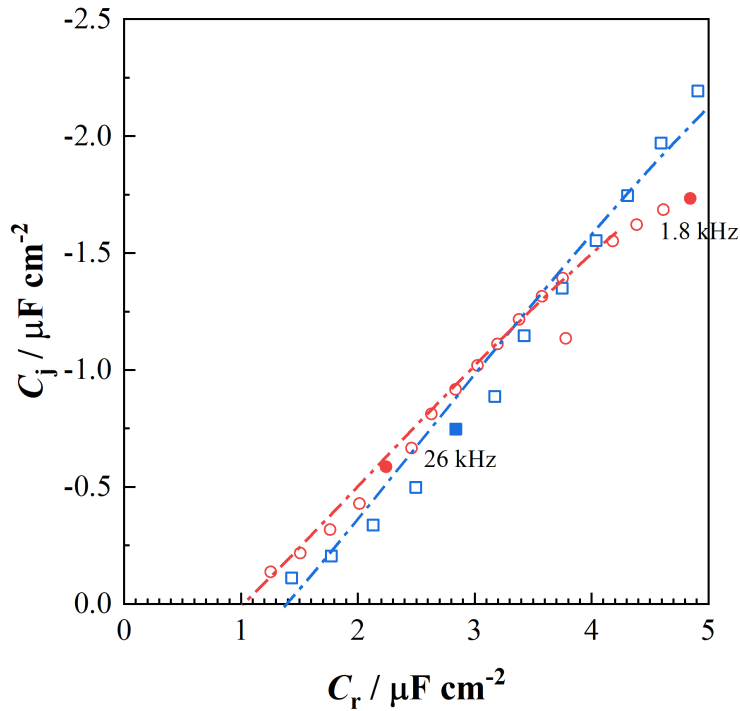
Figure 10: HF domain of the complex capacitance representation for an Al electrode after 2-hour immersion in 0.01 M Na₂SO₄ deaerated solution at the corrosion potential (E_{corr} = -1.196 V/MSE), calculated from the experimental impedance data presented in Figure 8. Red circles: raw data; blue squares: data corrected from the double layer CPE. Dashed lines are used for high frequency extrapolation of the capacitance.

4. CONCLUSIONS

This work shows that the different capacitances of an electrode can be readily obtained from a rather simple graphical analysis. However, depending on the value of the time constants, the frequency domains on which data analysis has to be performed, overlap.

The hypothesis of neglecting the double-layer capacitance compared to that of a thin film, such as a passive oxide film on an electrode, gives a good approximation of the characteristics of the thin layer. However, since all these capacitances usually show a frequency dispersion, it may be difficult to correctly evaluate the high-frequency limit of the complex capacitance graph. Furthermore, this work shows that it is possible to extract the double-layer capacitance by analyzing the low frequency part of the impedance diagram in order to use it for a more refined analysis of the high frequency domain of the diagram. It should be noted that no assumptions were made about the nature of the medium, making this approach applicable to other systems,

such as non-aqueous media and ionic liquids, and that the film thickness can be obtained without any assumption on the physical origin of the CPE.

In addition, it has been shown that the shape of the various graphical representations and in particular their extrapolation into the high-frequency domain is of great help to roughly assess the error that can be made and to give an overview of the frequency domain that can be exploited for the analysis of interfacial capacitance.

5. ACKNOWLEDGEMENTS

REFERENCES

[1] D. C. Grahame, *Chem Rev*. **1947**, *41*, 441-501.

[2] K. Shahzad, S. A. Lone, C. C. Mardare, A. I. Mardare, A. W. Hassel, *Electrochim. Acta*. **2021**, *367*.

[3] J. Han, H. L. Chan, M. G. Wartenberg, H. H. Heinrich, J. R. Scully, *Electrochem. Commun.* **2021**, *122*.

[4] S. Marcelin, B. Ter-Ovanessian, B. Normand, *Electrochem. Commun.* **2016**, *66*, 62-65.

[5] P. Córdoba-Torres, *Electrochim. Acta*. **2018**, *282*, 892-904.

[6] B. A. Yezer, A. S. Khair, P. J. Sides, D. C. Prieve, *J Colloid Interface Sci*. **2015**, *449*, 2-12.

[7] K. J. Aoki, J. Chen, R. He, *ACS Omega*. **2020**, *5*, 7497-7502.

[8] A. Allagui, T. J. Freeborn, A. S. Elwakil, B. J. Maundy, *Sci Rep*. **2016**, *6*, 38568.

[9] M. E. Orazem, I. Frateur, B. Tribollet, V. Vivier, S. Marcelin, N. Pebere, A. L. Bunge, E. A. White, D. P. Riemer, M. Musiani, *J. Electrochem. Soc.* **2013**, *160*, C215-C225.

[10] P. Zoltowski, *J. Electroanal. Chem.* **1998**, *443*, 149-154.

[11] M. H. Martin, A. Lasia, *Electrochim. Acta*. **2011**, *56*, 8058-8068.

[12] P. Charoen-amornkitt, T. Suzuki, S. Tsushima, *J. Electrochem. Soc.* **2020**, *167*.

[13] P. Córdoba-Torres, T. J. Mesquita, R. P. Nogueira, *J. Phys. Chem. C*. **2015**, *119*, 4136-4147.

[14] G. J. Brug, A. L. G. Vandeneeden, M. Sluytersrehbach, J. H. Sluyters, *J. Electroanal. Chem.* **1984**, *176*, 275-295.

[15] A. Sadkowski, *J. Electroanal. Chem.* **2000**, *481*, 222-226.

[16] S. P. Harrington, T. M. Devine, *J. Electrochem. Soc.* **2008**, *155*, C381-C386.

[17] S. P. Harrington, F. Wang, T. M. Devine, *Electrochim. Acta*. **2010**, *55*, 4092-4102.

[18] F. La Mantia, H. Habazaki, M. Santamaria, F. Di Quarto, *Russ. J. Electrochem.* **2010**, *46*, 1306-1322.

[19] R. Raccichini, L. Furness, J. W. Dibden, J. R. Owen, N. García-Araez, *J. Electrochem. Soc.* **2018**, *165*, A2741-A2749.

[20] J. Landesfeind, J. Hattendorff, A. Ehrl, W. A. Wall, H. A. Gasteiger, *J. Electrochem. Soc.* **2016**, *163*, A1373-A1387.

[21] J. M. Elliott, J. R. Owen, *Phys. Chem. Chem. Phys.* **2000**, *2*, 5653-5659.

[22] T. F. Esterle, D. Sun, M. R. Roberts, P. N. Bartlett, J. R. Owen, *Phys. Chem. Chem. Phys.* **2012**, *14*, 3872-3881.

[23] N. Meddings, M. Heinrich, F. Overney, J.-S. Lee, V. Ruiz, E. Napolitano, S. Seitz, G. Hinds, R. Raccichini, M. Gaberšček, J. Park, *J. Power Sources*. **2020**, *480*.

[24] J.-M. Atebamba, J. Moskon, S. Pejovnik, M. Gaberscek, *J. Electrochem. Soc.* **2010**, *157*.

[25] B. Ramezanzadeh, E. Ghasemi, M. Mahdavian, E. Changizi, M. H. Mohamadzadeh Moghadam, *Carbon.* **2015**, *93*, 555-573.

[26] K. A. Yasakau, J. Carneiro, M. L. Zheludkevich, M. G. S. Ferreira, *Surf. Coat. Tech.* **2014**, *246*, 6-16.

[27] K. A. Yasakau, A. Kuznetsova, S. Kallip, M. Starykevich, J. Tedim, M. G. S. Ferreira, M. L. Zheludkevich, *Corros. Sci.* **2018**, *143*, 299-313.

[28] A. J. Bard, L. R. Faulkner, Electrochemical Methods: Fundamentals and Applications, John Wiley & Sons New York, **2001**.

[29] M. E. Orazem, B. Tribollet, Electrochemical Impedance Spectroscopy, Wiley, Hoboken, New Jersey, **2017**.

[30] B. Hirschorn, M. E. Orazem, B. Tribollet, V. Vivier, I. Frateur, M. Musiani, *Electrochim. Acta.* **2010**, *55*, 6218-6227.

[31] M. Benoit, C. Bataillon, B. Gwinner, F. Miserque, M. E. Orazem, C. M. Sanchez-Sanchez, B. Tribollet, V. Vivier, *Electrochim. Acta.* **2016**, *201*, 340-347.

[32] S. Chakri, I. Frateur, M. E. Orazem, E. M. M. Sutter, T. T. M. Tran, B. Tribollet, V. Vivier, *Electrochim. Acta.* **2017**, *246*, 924-930.

[33] S. Chakri, A. N. Patel, I. Frateur, F. Kanoufi, E. M. M. Sutter, T. T. M. Tran, B. Tribollet, V. Vivier, *Anal. Chem.* **2017**, *89*, 5303-5310.

[34] C. Y. Chao, L. F. Lin, D. D. Macdonald, *J. Electrochem. Soc.* **2019**, *129*, 1874-1879.

[35] D. D. Macdonald, *J. Electrochem. Soc.* **1992**, *139*, 3434-3449.

[36] M. Bojinov, P. Kinnunen, K. Lundgren, G. Wikmark, *J. Electrochem. Soc.* **2005**, *152*, B250.

[37] I. Betova, M. Bojinov, P. Kinnunen, K. Lundgren, T. Saario, *J. Electrochem. Soc.* **2008**, *155*, C81.

[38] G. Tranchida, M. Clesi, F. Di Franco, F. Di Quarto, M. Santamaria, *Electrochim. Acta.* **2018**, *273*, 412-423.

[39] L. G. Bland, K. Gusieva, J. R. Scully, *Electrochim. Acta.* **2017**, *227*, 136-151.

[40] X. Dominguez-Benetton, S. Sevda, K. Vanbroekhoven, D. Pant, *Chem Soc Rev.* **2012**, *41*, 7228-7246.

[41] P. Visser, H. Terryn, J. M. C. Mol, *Corros. Sci.* **2018**, *140*, 272-285.

[42] P. Visser, M. Meeusen, Y. Gonzalez-Garcia, H. Terryn, J. M. C. Mol, *J. Electrochem. Soc.* **2017**, *164*, C396-C406.

[43] V. M.-W. Huang, V. Vivier, M. E. Orazem, N. Pebere, B. Tribollet, *J. Electrochem. Soc.* **2007**, *154*, C81-C88.

[44] V. M.-W. Huang, V. Vivier, I. Frateur, M. E. Orazem, B. Tribollet, *J. Electrochem. Soc.* **2007**, *154*, C89-C98.

[45] V. M.-W. Huang, V. Vivier, M. E. Orazem, N. Pebere, B. Tribollet, *J. Electrochem. Soc.* **2007**, *154*, C99-C107.

[46] O. Gharbi, A. Dizon, M. E. Orazem, M. T. T. Tran, B. Tribollet, V. Vivier, *Electrochim. Acta.* **2019**, *320*, 134609.

[47] P. Agarwal, M. E. Orazem, L. H. Garci-Rubio, *J. Electrochem. Soc.* **1992**, *139*, 1917-1927.

[48] P. Agarwal, M. E. Orazem, L. H. Garcia-Rubio, *J. Electrochem. Soc.* **1995**, *142*, 4159-4168.

[49] B. Hirschorn, M. E. Orazem, B. Tribollet, V. Vivier, I. Frateur, M. Musiani, *J. Electrochem. Soc.* **2010**, *157*, C452-C457.

[50] B. Hirschorn, M. E. Orazem, B. Tribollet, V. Vivier, I. Frateur, M. Musiani, *J. Electrochem. Soc.* **2010**, *157*, C458-C463.

[51] Y. M. Chen, A. S. Nguyen, M. E. Orazem, B. Tribollet, N. Pebere, M. Musiani, V. Vivier, *Electrochim. Acta.* **2016**, *219*, 312-320.

[52] S. Marcelin, Z. Zhang, B. Ter-Ovanessian, B. Normand, *J. Electrochem. Soc.* **2021**, *168*.

[53] T. T. M. Tran, B. Tribollet, E. M. M. Sutter, *Electrochim. Acta.* **2016**, *216*, 58-67.

[54] J. Evertsson, F. Bertram, F. Zhang, L. Rullik, L. R. Merte, M. Shipilin, M. Soldemo, S. Ahmadi, N. Vinogradov, F. Carlà, J. Weissenrieder, M. Göthelid, J. Pan, A. Mikkelsen, J. O. Nilsson, E. Lundgren, *Appl. Surf. Sci.* **2015**, *349*, 826-832.

[55] C. H. Hsu, F. Mansfeld, *Corrosion.* **2001**, *57*, 747-748.

[56] J. W. Schultze, M. M. Lohrengel, *Electrochim. Acta.* **2000**, *45*, 2499-2513.